Transparent, Flexible, All-Reduced Graphene Oxide Thin Film Transistors

Qiyuan He,[†] Shixin Wu,[†] Shuang Gao,[†] Xiehong Cao,[†] Zongyou Yin,[†] Hai Li,[†] Peng Chen,[‡] and Hua Zhang[†,§,*]

[†]School of Materials Science and Engineering, Nanyang Technological University, 50 Nanyang Avenue, Singapore 639798, Singapore, [‡]School of Chemical and Biomedical Engineering, Nanyang Technological University, 70 Nanyang Drive, Singapore 637457, Singapore, and [§]Centre for Biomimetic Sensor Science, Nanyang Technological University, 50 Nanyang Drive, Singapore 637553, Singapore

ABSTRACT Owing to their unique thickness-dependent electronic properties, together with perfect flexibility and transparency, graphene and its relatives make fantastic material for use in both active channel and electrodes in various electronic devices. On the other hand, the electronic sensors based on graphene show high potential in detection of both chemical and biological species with high sensitivity. In this contribution, we report the fabrication of all-reduced graphene oxide (rGO) thin film transistors by a combination of solution-processed rGO electrodes with a micropatterned rGO channel, and then study their applications in biosensing. Our all-rGO devices are cost-effective, highly reproducible, and reliable. The fabricated electronic sensor is perfectly flexible with high transparency, showing good sensitivity in detecting proteins in the physiological buffer. As a proof of concept, fibronectin as low as 0.5 nM was successfully detected, which is comparable with the previously reported protein sensors based on single-layer pristine graphene obtained from mechanical cleavage. The specific detection of avidin by using biotinylated all-rGO sensor is also successfully demonstrated.

KEYWORDS: reduced graphene oxide · field-effect transistors · protein detection · nanoelectronic sensing

Detection of biomolecules or biosignals *in vitro* and/or *in vivo* requires advanced sensors with high flexibility for the complex recording in three-dimensional conformation, as well as high transparency for optical observation and registration. To meet these requirements, thin film transistors (TFTs), based on networks of carbon nanotubes (CNTs)[1,2] and silicon nanowires (SiNWs),[3−5] and various organic TFTs (OTFTs)[6−9] have been intensively studied, which showed promising sensing applications in detection of various chemicals and biomolecules. However, the synthesis of CNTs and SiNWs often requires high-cost, complicated, and high-temperature chemical vapor deposition (CVD) techniques, which are not compatible with plastic substrates. On the other hand, OTFTs have suffered from intrinsic chemical and thermal instability due to the use of organic or polymeric materials.

Recently, graphene[10,11] and its derivatives[12−15] have emerged as promising channel materials in a number of electronics applications.[16−25] The excellent flexibility, chemical stability, and biocompatibility[26,27] render graphene an ideal channel material for advanced sensing applications.[21,24,25,28] Sensors based on graphene and its derivatives, prepared from the mechanical cleavage,[16,29,30] and thermal growth,[19,31] as well as reduced graphene oxide (rGO),[32−35] have shown potential in the detection of gas,[16,32−34] metal ions,[25] biomolecules,[30,35−38] and most recently biosignals of living cells.[21,29] Currently, the chemically reduced graphene oxide is widely used because of its unique advantages, such as low cost, mass production, facile solution process, and easy functionalization, *etc.*

As known, most of the reported plastic electronics still rely on the traditional electrodes, such as metals[1,3,39] or indium tin oxide (ITO) thin films,[40] but the graphene-based thin film, either from thermal growth or solution process,[41,42] has served as flexible electrodes[43,44] in various optical and electronic applications such as solar cells,[20,45] organic light emitting diodes (OLEDs),[46] and field-effect transistors (FETs),[47,48] where the graphene-based electrodes satisfied both high flexibility and transparency, resulting in the superior performance than that of the CNT networks[49] and giving competitive results with other high-cost approach generated materials, such as metal nanowire networks.[50]

In this contribution, we report a very simple method for fabrication of flexible and transparent all-rGO TFTs on polyethylene terephthalate (PET) substrates. The thick rGO film (>9 nm) on PET, obtained by a spin-coating method, is used as electrodes. The patterned thin rGO films (2−4 nm), obtained by the microfluidic method, are used as the active channel. The fabricated all-rGO device showed high transparency and superior flexibility toward bending, as well as highly reproducible field-effect and

* Address correspondence to hzhang@ntu.edu.sg.

Received for review March 24, 2011 and accepted April 27, 2011.

Published online April 27, 2011
10.1021/nn201118c

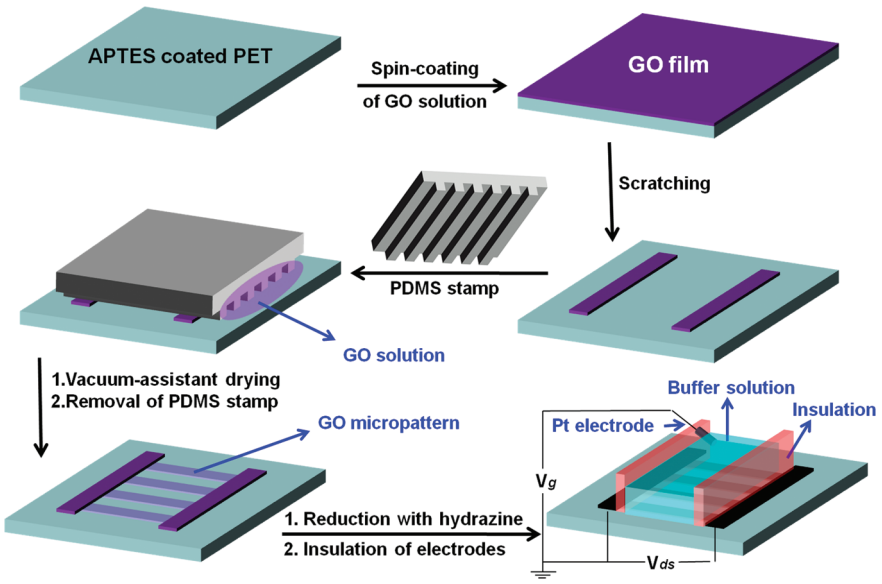

Figure 1. Schematic illustration for fabrication of all-rGO TFT.

sensing behaviors. As a proof of concept, we explore the application of the fabricated all-rGO TFTs in electronic biosensing for highly sensitive and selective protein detection.

RESULTS AND DISCUSSION

Figure 1 shows how to fabricate the all-rGO TFT. First, the graphene oxide (GO) solution was spin-coated onto a 3-aminopropyltriethoxysilane (APTES)-modified PET substrate.[21,51] The modification of APTES can enhance the adsorption of GO sheets on PET.[52] Then, a sharp plastic tip was used to scratch the GO film to fabricate two separated GO pads.[53] After that, the GO films were micropatterned between the two GO pads using the microfluidics technique.[21,54] The GO films on PET substrates were reduced with hydrazine vapor to obtain rGO films.[52] Finally, the silicone rubber was used to insulate two rGO electrodes, as drain and source, respectively, and to define the buffer-containing chamber for electrolyte-gating. The length of rGO electrodes and the distance between the rGO electrodes were fixed at 10 and 5 mm, determining the width and length of the conducting channel, respectively.

The detailed characterization of the rGO thin film is provided in the Supporting Information (SI). The patterned rGO films are uniform over a large area (Figure S1 in SI), consistent with our previous result,[21] which are essential for the reliable and reproducible device performance. The thickness of rGO electrodes was fixed at 8−10 nm, controlled by the volume of GO solution used in the spin-coating process (SI, Figure S2). The thickness of the rGO channel was fixed at 2−4 nm (*ca.* 2−4 layers of rGO sheets) by choosing the suitable concentration of GO solution supplied to the microfluidic channel (Figure S2). The well-controlled thin rGO channel is crucial toward both the sensitivity and reliability of fabricated TFTs in the following sensing experiments.

To obtain high conductivity while retaining the high transparency of rGO films, during our experiment, we varied the thickness of rGO electrodes from 3 to 12 nm to investigate how the thickness of rGO electrodes affects the device performance. SI, Figure S3A shows the dependence of the transmittance, measured at wavelength of 550 nm, and the overall resistance of the TFT device on the thickness of the rGO electrodes (each resistance value was obtained by averaging the experimental data measured in five devices). When the thickness of rGO channel was fixed at 2−4 nm, we found that the conductance of TFT increased with the thickness of rGO electrodes. If the thickness of rGO electrodes is ~3 nm, the conductance of TFT is rather low (resistance of *ca.* 28 MΩ), which arises from the discontinuous rGO thin films, but it gives a high transparency (>85% at 550 nm). In this case, the measured device noise becomes dominant and the detection sensitivity would be low. No obvious improvement in resistance (within 5%) was observed when the thickness of rGO electrodes exceeds 9 nm. Therefore, 9 nm thick rGO electrodes were chosen in the following experiments in order to satisfy both conductance (<2 MΩ) and transparency (>75%).

Supporting Information, Figure S3B shows the transmittance of all-rGO TFT on PET in the visible range, confirming its high transparency (90% at rGO channel region and 75% at rGO electrode). This is in agreement with the previous reports on rGO electrodes used for solar cells.[17,20]

The field-effect characteristic was tested with electrolyte-gating in a PBS buffer solution (pH 7.2). Figure 2A shows a typical plot of drain−source current (I_{ds}) *vs* electrolyte-gate voltage (V_g) in the fabricated all-rGO

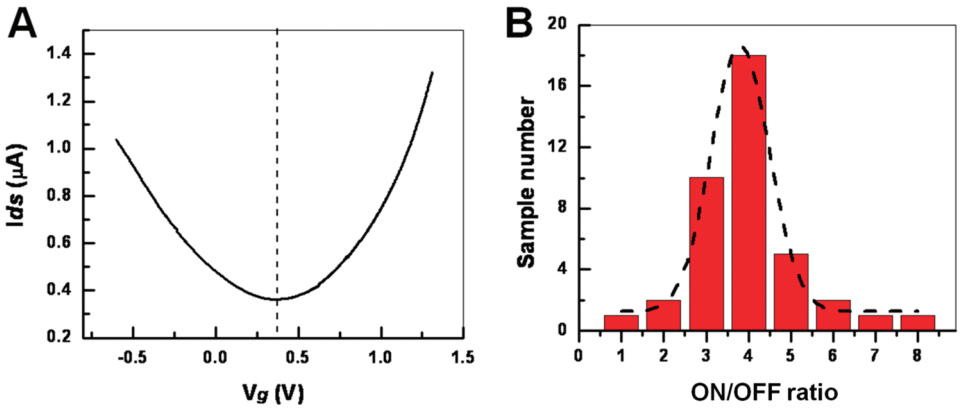

Figure 2. (A) A typical $I_{ds}-V_g$ curve (drain−source current *vs* electrolyte-gate voltage) in a PBS buffer solution at $V_{ds} = 400$ mV. (B) Distribution of ON/OFF ratio measured in 40 devices. ON/OFF ratio was obtained from V_g in the range from −0.5 to 1.2 V.

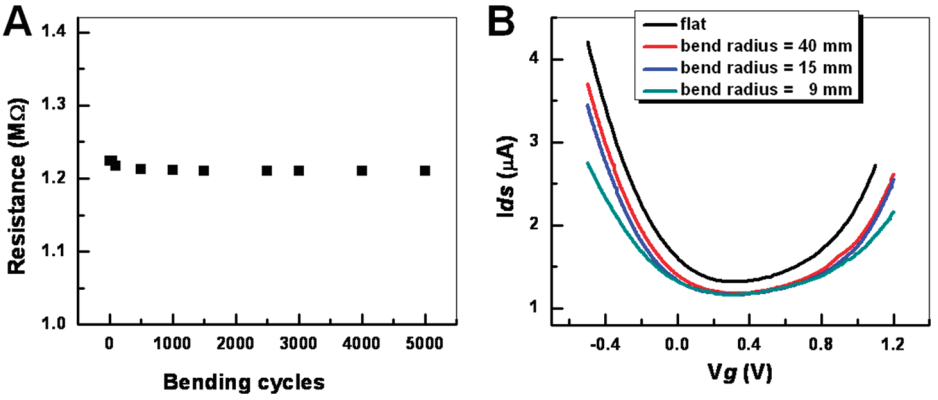

Figure 3. (A) Bending experiments of one all-rGO TFT. The bend radius is 4 mm. (B) $I_{ds}-V_g$ curve in a PBS buffer solution at different bend radius at $V_{ds} = 400$ mV.

TFT. The typical ambipolar characteristics were observed in all fabricated devices. In contrast to the single-layer graphene-based FETs whose performance often varies largely from batch to batch, our devices showed stable and consistent performance. The Dirac point is at $+0.4 \pm 0.1$ V. Unlike the sharp transition in the Dirac point of the pristine graphene-based devices,[31,55] the all-rGO device exhibited a rather smooth transition. Figure 2B shows the distribution of the ON/OFF ratio obtained from 40 all-rGO devices with fixed width (10 mm) and length (5 mm) of the rGO channel. The average ON/OFF ratio is 3.8 ± 0.7 (Figure 2B). All these results indicate that the all-rGO devices preserve the similar field-effect properties as shown in the rGO or graphene-based FETs with common metal electrodes (*e.g.,* Au and Ag).[21,29]

Figure 3A shows that there is no obvious resistance increase in the all-rGO TFT on PET with increasing the bending cycles (even after 5,000 bending cycles) at the bend radius of 4 mm, suggesting that the all-rGO TFT device has an excellent flexibility. The resistance of the device decreased about 1% after the initial 200-time bending cycles and became stable afterward. It may arise from the rearrangement of rGO sheets during the initial bending, which enhanced the intimate stacking of rGO layers.

To investigate how the bending affects the transistor behavior, the electrical property of all-rGO TFT at different bending radius was investigated. The resistance of TFT increased with bend radius (ca. 24% at bend radius of 9 mm, SI, Figure S4). Figure 3B shows the plot of I_{ds} *vs* V_g at different bending radius. The bending has not resulted in the obvious shift of transconductance. However, it broadened the transition region around the Dirac point and lowered the ON/OFF ratio from 3.4 to 2.4 at bend radius of 9 mm.

As mentioned above, the fabricated all-rGO TFTs showed excellent reproducibility, flexibility, and transparency, which could have promising applications in electronic sensing. As a proof of concept, we first applied the all-rGO TFTs to real-time detect the nonspecific absorption of fibronectin in buffer solution. The rGO channel was first functionalized with 1-pyrenebutanoic acid succinimidyl ester (*i.e.*, carboxyl group-terminated pyrene), which served as the linker molecule to catch proteins in buffer solution. As shown in Figure 4A, the cross-linking of fibronectin onto the functionalized rGO channel resulted in the decrease of current. Figure 4B gives the percentage change of I_{ds} as a function of fibronectin concentration, confirming that fibronectin as low as 0.5 nM was successfully

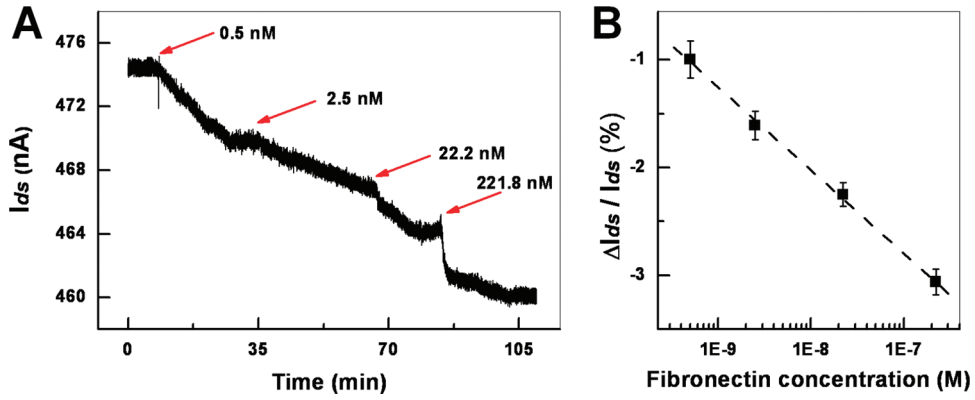

Figure 4. (A) Real-time detection of fibronection with increasing concentration in PBS buffer by using the pyrene-functionalized all-rGO TFT sensor. (B) The plot of current change *vs* fibronectin concentration. The standard error in each concentration was obtained by measuring five samples.

detected with a signal-to-noise ratio of 16. This detect limit is comparable with the reported result obtained by the single-layer pristine graphene-based protein sensors.[30]

To study the biosensing selectivity, we further applied the all-rGO sensor to real-time detection of the specific binding of biotin−avidin by the biotinylated rGO channel, where the polyethyleneimine (PEI) coating was used to link biotin and polyethylene glycol (PEG) coating was used to prevent the nonspecific binding of proteins. Figure 5A shows the real-time measurement of I_{ds} while avidin with increasing concentration was introduced to the PEI/PEG coated-rGO TFT with biotinylation. The binding of avidin through the strong biotin−avidin interaction on the rGO channel resulted in the increase of I_{ds}. The current began to increase within 2 s after addition of avidin and continued to increase for 10−25 min until it reached a stable value, indicating the saturation of the adsorption of avidin on the biotinylated rGO channel. Note that during addition of the target solution, sometimes the current immediately jumped to a higher level, mostly likely due to the disturbance to the solution in the sensing chamber. A lowest avidin concentration of 80 nM was detected at a signal-to-noise ratio of 3 (inset in Figure 5A). The introduction of bovine serum albumin (BSA) did not result in the change of current (inset in Figure 5A), which confirmed that the PEG-coating successfully prevented the nonspecific absorption of proteins. Figure 5B shows the steady-state percentage change of I_{ds} as a function of avidin concentration.

The mechanism of such current change upon binding of target molecules can be explained by the direct doping effect instead of the electrostatic gating effect. Since the isoelectric point of fibronectin and avidin is 5 and 10.5, respectively. Electrostatic gating from the negatively charged fibronectin would predict a positive-shift of the Dirac point in $I_{ds}-V_g$, while the positively charged avidin would produce a negative-shift. However, as shown in Figure 6, the opposite trends were observed in both cases. Therefore, the current response could be attributed to the n-doping effect from fibronectin and the p-doping effect from avidin.

In summary, TFTs with rGO as both channel (2−4 nm thick rGO micropatterns) and electrode materials (*ca.* 9 nm thick rGO pads) have been successfully fabricated by a simple method. Such all-rGO devices are perfectly flexible with good transparency. The typical ambipolar field-effect characteristics with ON/OFF ratio of 3.8 and Dirac point of +0.4 V in the electrolyte-gating is reliably observed in more than 40 devices. As a proof-of-concept biosensor, the all-rGO TFT showed good sensitivity and selectivity in protein detection. Our promising results suggest that the solution processed rGO is an excellent material, which could be used in flexible electronics, in particular, the flexible electronic sensors with high sensitivity and selectivity.

MATERIALS AND METHODS

Fabrication of All-Reduced Graphene Oxide (rGO) Thin Film Transistors (TFTs). Figure 1 shows the schematic illustration for fabrication of all-rGO TFTs. The substrates used in our experiments, for example, PET and SiO_2 substrates, were first modified with 3-aminopropyltriethoxysilane (APTES, Sigma) self-assembled monolayers (SAMs),[51] in order to enhance the adsorption of graphene oxide (GO) films. The fabrication process is described as follows. First, the GO solution in methanol (0.5 mg/mL)[17,53] was spin-coated on the APTES-modified substrates at 4000 rpm. The thickness of spin-coated GO film was controlled by the volume of GO solution. Typically, after 150 μL of 0.5 mg/mL GO solution were spin-coated (15 μL/drop) on the APTES-coated PET substrate, *ca.* 9 nm rGO film was obtained after chemical reduction of the obtained GO film on PET. The drain and source electrodes with size of 2 × 10 mm^2 were created by the previously reported scratching method[53] with a sharp plastic tip. Second, a microfluidics-based micropatterning technique[21,54] was applied to generate

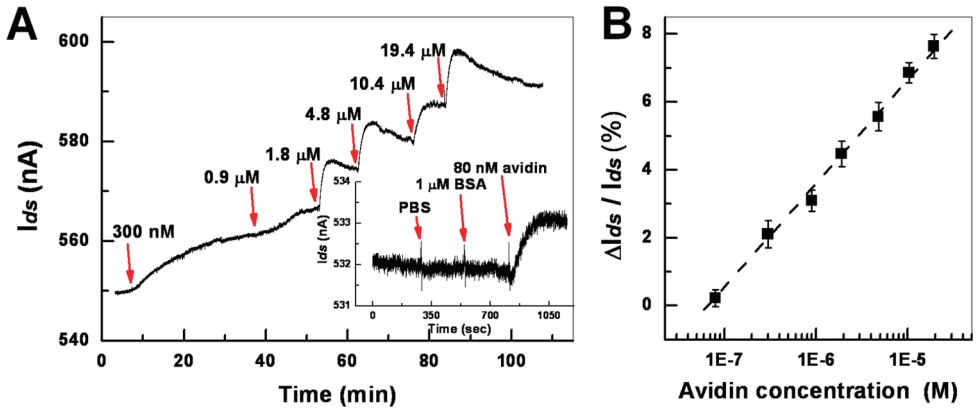

Figure 5. (A) Real-time specific detection of avidin with increasing concentration in PBS buffer by using the biotinylated all-rGO TFT sensor. Inset: Current response of biotinylated sensor to addition of PBS buffer, 1 μM BSA, and 80 nM avidin. (B) The plot of current change *vs* avidin concentration. The standard error in each concentration was obtained by measuring five samples.

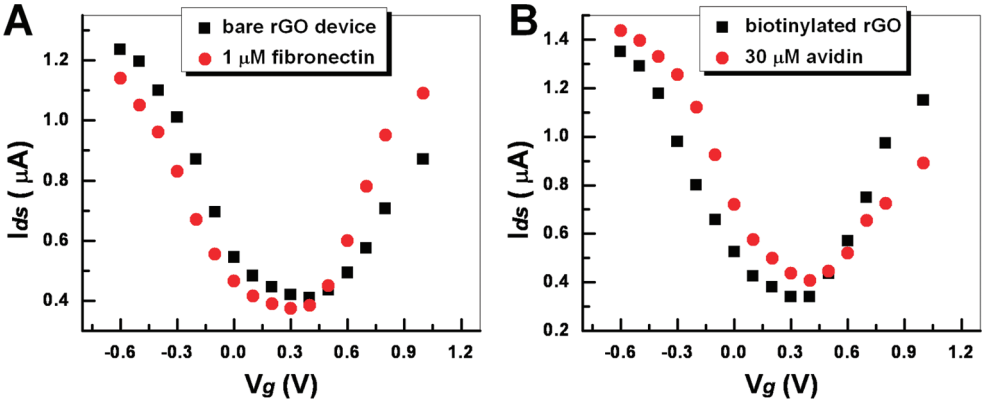

Figure 6. (A) I_{ds}–V_g curves of all-rGO TFTs before and after binding of fibronectin. (B) I_{ds}–V_g curves of biotinylated all-rGO TFTs before and after binding of avidin.

thin GO micropatterns between two GO pads. As shown in Figure 1, an O_2 plasma-treated PDMS stamp with line channels (10 μm width, 5 μm height, and 10 mm length) was placed on the APTES-modified substrate and perpendicular to the two GO pads to form close contact. A drop (10 μL) of GO aqueous solution (2 mg/mL) was then dropped at one end of the PDMS stamp to allow the GO solution to flow through the PDMS stamp channels. After drying in vacuum oven for 30 min, the PDMS stamp was carefully removed and the GO micropatterns were formed between two GO pads, which were reduced in hydrazine vapor at 60 °C for 12 h[52] to form rGO electrodes and rGO channel. Silicone rubber (Dow Corning) was used to insulate the contacted areas between rGO channel and rGO electrodes to define the sensor chamber.

The resulting rGO electrodes and micropatterns were characterized by optical microscopy and atomic force microscopy (AFM). Optical images were recorded with Nikon Eclipse LV100 optical microscopy. AFM images were obtained by using Dimension 3100 (Veeco, CA) in tapping mode with a Si tip (Veeco, resonant frequency, 320 kHz; spring constant, 42 N/m) under ambient conditions with a scanning rate of 1 Hz and scanning line of 512.

Electric Measurement. Electrical property of the resulting all-rGO TFTs was measured using a semiconductor device analyzer (Agilent B1500A). The length of rGO conducting channel was fixed at 5 mm, which is determined by the distance between the drain and source rGO electrodes. The width of patterned rGO channel is fixed at 10 mm, which is determined by the length of the rGO electrodes with size of 2 × 10 mm^2. At a fixed drain–source bias (V_{ds}) of 400 mV, the drain–source current (I_{ds}) was continuously measured while varying the electrolyte-gating potential (V_g) applied through the Pt electrode in a PBS buffer solution (pH 7.2).

Detection of Fibronection. The rGO channel was immersed into a DMF solution of 1-pyrenebutanoic acid succinimidyl ester (10 mM) for 4 h, followed by thorough rinsing with DI water and drying with N_2. The obtained device was used for biosensing application. The electric measurement was carried out by continuously monitoring the drain–source current (I_{ds}), while the fibronectin solution (Sigma, 1 μL of 100 nM, 0.4 μM, 4 μM, 40 μM) was continuously introduced into 200 μL PBS buffer solution (pH 7.2) in the sensor chamber, in order to test the total concentration of fibronetin in buffer solution (*i.e.*, 0.5, 2.5, 22.2, and 218.1 nM).

Detection of Avidin. The rGO channel was immersed into a mixed solution of 10 wt % of polyethyleneimine (PEI, average molecular weight 25000, Sigma) and 10 wt % polyethylene glycol (PEG, average molecular weight 6000, Sigma) for 4 h, followed by thorough rinsing with DI water. After the PEI/PEG coating, the rGO channel was biontinylated after immersing in a 10 mM DMF solution of biotin-*N*-hydroxysuccinimide ester (Sigma) overnight, followed by rinsing with DMF and DI water and drying with N_2. The electric measurement was carried out by continuously monitoring the drain–source current (I_{ds}), while the avidin solution (Sigma, 1 μL, 2 μL of 90 μM, and 1 μL, 3 μL, 6 μL, 10 μL of 300 μM) was continuously introduced into 300 μL PBS buffer solution (pH 7.2) in the sensor chamber, in order to test the total concentration of avidin in buffer solution (i.e., 0.3, 0.9, 1.9, 4.8, 10.4, and 19.4 μM).

Acknowledgment. This work was supported by AcRF Tier 2 (ARC 10/10, No. MOE2010-T2-1-060) from MOE, CRP (NRF-CRP2-2007-01) from NRF, A*STAR SERC Grants (No. 092 101 0064 and No. 072 101 0020) from A*STAR, CREATE program (Nanomaterials for Energy and Water Management) from NRF, and New Initiative Fund FY 2010 (M58120031) from NTU in Singapore.

Supporting Information Available: Characterization of fabricated rGO electrodes and micropatterns on Si/SiO_2 substrate (Figure S1, S2). The dependence of transmittance and device resistance of TFTs on the thickness of rGO electrodes (Figure S3). The $I_{ds}-V_{ds}$ characteristics measured at different bend radii (Figure S4). This material is available free of charge *via* the Internet at http://pubs.acs.org.

REFERENCES AND NOTES

1. Cao, Q.; Kim, H.; Pimparkar, N.; Kulkarni, J. P.; Wang, C.; Shim, M.; Roy, K.; Alam, M. A.; Rogers, J. A. Medium-Scale Carbon Nanotube Thin-Film Integrated Circuits on Flexible Plastic Substrates. *Nature* **2008**, *454*, 495–500.
2. Kang, S. J.; Kocabas, C.; Ozel, T.; Shim, M.; Pimparkar, N.; Alam, M. A.; Rotkin, S. V.; Rogers, J. A. High-Performance Electronics Using Dense, Perfectly Aligned Arrays of Single-Walled Carbon Nanotubes. *Nat. Nanotechnol.* **2007**, *2*, 230–236.
3. Cohen-Karni, T.; Timko, B. P.; Weiss, L. E.; Lieber, C. M. Flexible Electrical Recording from Cells Using Nanowire Transistor Arrays. *Proc. Natl. Acad. Sci. U.S.A.* **2009**, *106*, 7309–7313.
4. Timko, B. P.; Cohen-Karni, T.; Yu, G. H.; Qing, Q.; Tian, B. Z.; Lieber, C. M. Electrical Recording from Hearts with Flexible Nanowire Device Arrays. *Nano Lett.* **2009**, *9*, 914–918.
5. McAlpine, M. C.; Ahmad, H.; Wang, D.; Heath, J. R. Highly Ordered Nanowire Arrays on Plastic Substrates for Ultrasensitive Flexible Chemical Sensors. *Nat. Mater.* **2007**, *6*, 379–384.
6. Berggren, M.; Richter-Dahlfors, A. Organic Bioelctronics. *Adv. Mater.* **2007**, *19*, 3201–3213.
7. Someya, T.; Sekitani, T.; Iba, S.; Kato, Y.; Kawaguchi, H.; Sakurai, T. A Large-Area, Flexible Pressure Sensor Matrix with Organic Field-Effect Transistors for Artificial Skin Applications. *Proc. Natl. Acad. Sci. U.S.A.* **2004**, *101*, 9966–9970.
8. Mannsfeld, S. C. B.; Tee, B. C. K.; Stoltenberg, R. M.; Chen, C. V.; Barman, S.; Muir, B. V.; Sokolov, A. N.; Reese, C.; Bao, Z. Highly Sensitive Flexible Pressure Sensors with Microstructured Rubber Dielectric Layers. *Nat. Mater.* **2010**, *9*, 859–864.
9. Torsi, L.; Dodabalapur, A. Organic Thin-Film Transistors as Plastic Analytical Sensors. *Anal. Chem.* **2005**, *77*, 380 A–387A.
10. Novoselov, K. S.; Geim, A. K.; Morozov, S. V.; Jiang, D.; Zhang, Y.; Dubonos, S. V.; Grigorieva, I. V.; Firsov, A. A. Electric Field Effect in Atomically Thin Carbon Films. *Science* **2004**, *306*, 666–669.
11. Huang, X.; Yin, Z. Y.; Wu, S. X.; Qi, X. Y.; He, Q. Y.; Zhang, Q. C.; Yan, Q. Y.; Boey, F.; Zhang, H. Graphene-Based Materials: Synthesis, Characterization, Properties and Applications. *Small* **2011**, DOI: 10.1002/smll.201002009.
12. Li, X.; Cai, W.; An, J.; Kim, S.; Nah, J.; Yang, D.; Piner, R.; Velamakanni, A.; Jung, I.; Tutuc, E.; *et al.* Large-Area Synthesis of High-Quality and Uniform Graphene Films on Copper Foils. *Science* **2009**, *324*, 1312–1314.
13. Berger, C.; Song, Z. M.; Li, X. B.; Wu, X. S.; Brown, N.; Naud, C.; Mayou, D.; Li, T. B.; Hass, J.; Marchenkov, A. N.; *et al.* Electronic Confinement and Coherence in Patterned Epitaxial Graphene. *Science* **2006**, *312*, 1191–1196.
14. Stankovich, S.; Piner, R. D.; Chen, X. Q.; Wu, N. Q.; Nguyen, S. T.; Ruoff, R. S. Stable Aqueous Dispersions of Graphitic Nanoplatelets *via* the Reduction of Exfoliated Graphite Oxide in the Presence of Poly(sodium 4-styrenesulfonate). *J. Mater. Chem.* **2006**, *16*, 155–158.
15. Gilje, S.; Han, S.; Wang, M.; Wang, K. L.; Kaner, R. B. A Chemical Route to Graphene for Device Applications. *Nano Lett.* **2007**, *7*, 3394–3398.
16. Schedin, F.; Geim, A. K.; Morozov, S. V.; Hill, E. W.; Blake, P.; Katsnelson, M. I.; Novoselov, K. S. Detection of Individual Gas Molecules Adsorbed on Graphene. *Nat. Mater.* **2007**, *6*, 652–655.
17. Yin, Z. Y.; Wu, S. X.; Zhou, X. Z.; Huang, X.; Zhang, Q. C.; Boey, F.; Zhang, H. Electrochemical Deposition of ZnO Nanorods on Transparent Reduced Graphene Oxide Electrodes for Hybrid Solar Cells. *Small* **2010**, *6*, 307–312.
18. Liu, W.; Jackson, B. L.; Zhu, J.; Miao, C.-Q.; Chung, C.-H.; Park, Y. J.; Sun, K.; Woo, J.; Xie, Y.-H. Large Scale Pattern Graphene Electrode for High Performance in Transparent Organic Single Crystal Field-Effect Transistors. *ACS Nano* **2010**, *4*, 3927–3932.
19. Dong, X. C.; Shi, Y. M.; Huang, W.; Chen, P.; Li, L.-J. Electrical Detection of DNA Hybridization with Single-Base Specificity Using Transistors Based on CVD-Grown Graphene Sheets. *Adv. Mater.* **2010**, *22*, 1649–1653.
20. Yin, Z. Y.; Sun, S.; Salim, T.; Wu, S. X.; Huang, X.; He, Q. Y.; Lam, Y. M.; Zhang, H. Organic Photovoltaic Devices Using Highly Flexible Reduced Graphene Oxide Films as Transparent Electrodes. *ACS Nano* **2010**, *4*, 5263–5268.
21. He, Q. Y.; Sudibya, H. G.; Yin, Z. Y.; Wu, S. X.; Li, H.; Boey, F.; Huang, W.; Chen, P.; Zhang, H. Centimeter-Long and Large-Scale Micropatterns of Reduced Graphene Oxide Films: Fabrication and Sensing Applications. *ACS Nano* **2010**, *4*, 3201–3208.
22. Liu, J. Q.; Lin, Z.; Liu, T.; Yin, Z. Y.; Zhou, X. Z.; Chen, S.; Xie, L. H.; Boey, F.; Zhang, H.; Huang, W. Multilayer Stacked Low-Temperature-Reduced Graphene Oxide Films: Preparation, Characterization, and Application in Polymer Memory Devices. *Small* **2010**, *6*, 1536–1542.
23. Liu, J. Q.; Yin, Z. Y.; Cao, X. H.; Zhao, F.; Ling, A.; Xie, L. H.; Fan, Q. L.; Boey, F.; Zhang, H.; Huang, W. Bulk Heterojunction Polymer Memory Devices with Reduced Graphene Oxide as Electrodes. *ACS Nano* **2010**, *4*, 3987–3992.
24. Cao, X. H.; He, Q. Y.; Shi, W. H.; Li, B.; Zeng, Z. Y.; Shi, Y. M.; Yan, Q. Y.; Zhang, H. Graphene Oxide as Carbon Source for Controlled Growth of Carbon Nanowires. *Small* **2011**, *7*, 1199–1202.
25. Sudibya, H. G.; He, Q. Y.; Zhang, H.; Chen, P. Electrical Detection of Metal Ions Using Field-Effect Transistors Based on Micropatterned Reduced Graphene Oxide Films. *ACS Nano* **2011**, *5*, 1990–1994.
26. Agarwal, S.; Zhou, X.; Ye, F.; He, Q.; Chen, G. C. K.; Soo, J.; Boey, F.; Zhang, H.; Chen, P. Interfacing Live Cells with Nanocarbon Substrates. *Langmuir* **2010**, *26*, 2244–2247.
27. Chen, H.; Müller, M. B.; Gilmore, K. J.; Wallace, G. G.; Li, D. Mechanically Strong, Electrically Conductive, and Biocompatible Graphene Paper. *Adv. Mater.* **2008**, *20*, 3557–3561.
28. Yang, W.; Ratinac, K.; Ringer, S.; Thordarson, P.; Gooding, J.; Braet, F. Carbon Nanomaterials in Biosensors: Should You Use Nanotubes or Graphene? *Angew. Chem., Int. Ed.* **2010**, *49*, 2114–2138.
29. Cohen-Karni, T.; Qing, Q.; Li, Q.; Fang, Y.; Lieber, C. M. Graphene and Nanowire Transistors for Cellular Interfaces and Electrical Recording. *Nano Lett.* **2010**, *10*, 1098–1102.
30. Ohno, Y.; Maehashi, K.; Yamashiro, Y.; Matsumoto, K. Electrolyte-Gated Graphene Field-Effect Transistors for Detecting pH and Protein Adsorption. *Nano Lett.* **2009**, *9*, 3318–3322.
31. Ang, P. K.; Chen, W.; Wee, A. T. S.; Loh, K. P. Solution-Gated Epitaxial Graphene as pH Sensor. *J. Am. Chem. Soc.* **2008**, *130*, 14392–14393.
32. Fowler, J. D.; Allen, M. J.; Tung, V. C.; Yang, Y.; Kaner, R. B.; Weiller, B. H. Practical Chemical Sensors from Chemically Derived Graphene. *ACS Nano* **2009**, *3*, 301–306.
33. Robinson, J. T.; Perkins, F. K.; Snow, E. S.; Wei, Z. Q.; Sheehan, P. E. Reduced Graphene Oxide Molecular Sensors. *Nano Lett.* **2008**, *8*, 3137–3140.
34. Dua, V.; Surwade, S. P.; Ammu, S.; Agnihotra, S. R.; Jain, S.; Roberts, K. E.; Park, S.; Ruoff, R. S.; Manohar, S. K. All-Organic Vapor Sensor Using Inkjet-Printed Reduced Graphene Oxide. *Angew. Chem., Int. Ed.* **2010**, *49*, 2154–2157.
35. Mao, S.; Lu, C. H.; Yu, K. H.; Bo, Z.; Chen, J. H. Specific Protein Detection Using Thermally Reduced Graphene Oxide

Sheet Decorated with Gold Nanoparticle−Antibody Conjugates. *Adv. Mater.* **2010**, *22*, 3521–3526.
36. Wang, Z.; Zhou, X.; Zhang, J.; Boey, F.; Zhang, H. Direct Electrochemical Reduction of Single-Layer Graphene Oxide and Subsequent Functionalization with Glucose Oxidase. *J. Phys. Chem. C* **2009**, *113*, 14071–14075.
37. He, S.; Song, B.; Li, D.; Zhu, C.; Qi, W.; Wen, Y.; Wang, L.; Song, S.; Fang, H.; Fan, C. A Graphene Nanoprobe for Rapid, Sensitive, and Multicolor Fluorescent DNA Analysis. *Adv. Funct. Mater.* **2010**, *20*, 453–459.
38. Wang, Z. J.; Zhang, J.; Chen, P.; Zhou, X. Z.; Yang, Y. L.; Wu, S. X.; Niu, L.; Han, Y.; Wang, L. H.; Chen, P.; *et al.* Label-Free, Electrochemical Detection of Methicillin-Resistant Staphylococcus Aureus DNA with Reduced Graphene Oxide-Modified Electrodes. *Biosens. Bioelectron.* **2011**, *26*, 3881–3886.
39. O'Connor, B.; Haughn, C.; An, K. H.; Pipe, K. P.; Shtein, M. Transparent and Conductive Electrodes Based on Unpatterned, Thin Metal Films. *Appl. Phys. Lett.* **2008**, *93*, 223304.
40. Kim, D.-H.; Park, M.-R.; Lee, H.-J.; Lee, G.-H. Thickness Dependence of Electrical Properties of ITO Film Deposited on a Plastic Substrate by RF Magnetron Sputtering. *Appl. Surf. Sci.* **2006**, *253*, 409–411.
41. Shuping, P.; Hoi Nok, T.; Xinliang, F.; Klaus, M. Patterned Graphene Electrodes from Solution-Processed Graphite Oxide Films for Organic Field-Effect Transistors. *Adv. Mater.* **2009**, *21*, 3488–3491.
42. Li, X.; Zhu, Y.; Cai, W.; Borysiak, M.; Han, B.; Chen, D.; Piner, R. D.; Colombo, L.; Ruoff, R. S. Transfer of Large-Area Graphene Films for High-Performance Transparent Conductive Electrodes. *Nano Lett.* **2009**, *9*, 4359–4363.
43. Wu, S. X.; Yin, Z. Y.; He, Q. Y.; Lu, G.; Zhou, X. Z.; Zhang, H. Electrochemical Deposition of Cl-Doped n-Type Cu_2O on Reduced Graphene Oxide Electrodes. *J. Mater. Chem.* **2011**, *21*, 3467–3470.
44. Wu, S. X.; Yin, Z. Y.; He, Q. Y.; Huang, X.; Zhou, X. Z.; Zhang, H. Electrochemical Deposition of Semiconductor Oxides on Reduced Graphene Oxide-Based Flexible, Transparent and Conductive Electrodes. *J. Phys. Chem. C.* **2010**, *114*, 11816–11821.
45. Gomez de Arco, L.; Zhang, Y.; Schlenker, C. W.; Ryu, K.; Thompson, M. E.; Zhou, C. Continuous, Highly Flexible, and Transparent Graphene Films by Chemical Vapor Deposition for Organic Photovoltaics. *ACS Nano* **2010**, *4*, 2865–2873.
46. Wu, J.; Agrawal, M.; Becerril, H. c. A.; Bao, Z.; Liu, Z.; Chen, Y.; Peumans, P. Organic Light-Emitting Diodes on Solution-Processed Graphene Transparent Electrodes. *ACS Nano* **2010**, *4*, 43–48.
47. Chen., Y; Xu, Y.; Zhao, K.; Wan, X.; Deng, J.; Yan, W. Towards Flexible All-Carbon Electronics: Flexible Organic Field-Effect Transistors and Inverter Circuits Using Solution-Processed All-Graphene Source/Drain/Gate Electrodes. *Nano Res.* **2010**, *3*, 714–721.
48. Wang, S.; Ang, P. K.; Wang, Z.; Tang, A. L. L.; Thong, J. T. L.; Loh, K. P. High Mobility, Printable, and Solution-Processed Graphene Electronics. *Nano Lett.* **2009**, *10*, 92–98.
49. Li, J.; Hu, L.; Wang, L.; Zhou, Y.; Grüner, G.; Marks, T. J. Organic Light-Emitting Diodes Having Carbon Nanotube Anodes. *Nano Lett.* **2006**, *6*, 2472–2477.
50. Lee, J.-Y.; Connor, S. T.; Cui, Y.; Peumans, P. Solution-Processed Metal Nanowire Mesh Transparent Electrodes. *Nano Lett.* **2008**, *8*, 689–692.
51. Li, H.; Zhang, J.; Zhou, X.; Lu, G.; Yin, Z.; Li, G.; Wu, T.; Boey, F.; Venkatraman, S. S.; Zhang, H. Amino Silane Micropatterns on Hydroxyl-Terminated Substrates: Fabrication and Applications. *Langmuir* **2010**, *26*, 5603–5609.
52. Zhou, X. Z.; Huang, X.; Qi, X. Y.; Wu, S. X.; Xue, C.; Boey, F. Y. C.; Yan, Q. Y.; Chen, P.; Zhang, H. *In Situ* Synthesis of Metal Nanoparticles on Single-Layer Graphene Oxide and Reduced Graphene Oxide Surfaces. *J. Phys. Chem. C* **2009**, *113*, 10842–10846.
53. Li, B.; Cao, X.; Ong, H. G.; Cheah, J. W.; Zhou, X.; Yin, Z.; Li, H.; Wang, J.; Boey, F.; Huang, W.; *et al.* All-Carbon Electronic Devices Fabricated by Directly Grown Single-Walled Carbon Nanotubes on Reduced Graphene Oxide Electrodes. *Adv. Mater.* **2010**, *22*, 3058–3061.
54. Yin, Z.; He, Q.; Huang, X.; Lu, G.; Hng, H. H.; Chen, H.; Xue, C.; Yan, Q.; Boey, F.; Zhang, Q.; *et al.* Generation of Dual Patterns of Metal Oxide Nanomaterials Based on Seed-Mediated Selective Growth. *Langmuir* **2010**, *26*, 4616–4619.
55. Das., A.; Pisana, S.; Chakraborty, B.; Piscanec, S.; Saha, S. K.; Waghmare, U. V.; Novoselov, K. S.; Krishnamurthy, H. R.; Geim, A. K.; Ferrari, A. C.; *et al.* Monitoring Dopants by Raman Scattering in an Electrochemically Top-Gated Graphene Transistor. *Nat. Nanotechnol.* **2008**, *3*, 210–215.